ELSEVIER

Polymer 42 (2001) 4233–4251

polymer

www.elsevier.nl/locate/polymer

Spatial variation of structural hierarchy in injection molded PVDF and blends of PVDF with PMMA. Part II. Application of microbeam WAXS pole figure and SAXS techniques

Y.D. Wang, M. Cakmak*

Polymer Engineering Institute, University of Akron, Akron, OH 44325-0301, USA

Received 20 June 2000; received in revised form 6 October 2000; accepted 9 October 2000

Abstract

The influence of blend composition on the processing–structure–property relationships in injection molded PVDF and blends of PVDF with PMMA was investigated. Local crystalline order and chain orientation were studied using newly developed microbeam wide angle X-ray pole figure camera. The depth profiling of lamellar texture was investigated using SAXS combined with microtomy. These techniques provided a general picture on the macro and microstructural spatial gradients developed in the injection molded parts as influenced by the process condition and the composition of the blends.

The injection molded PVDF samples were found to exhibit a typical three layer morphology. The skin layer is formed as a result of the extensional flow with dominant *c*-axis orientation along the flow direction (FD). The crystal lamellae in this region are mainly extended in the direction perpendicular to the FD. The "shear zone" formed under the shear flow possesses "shish–kebab" structure. The "shish" structure is formed under high shear stress with "kebab" lateral overgrowth that occurs at subsequent stages. The chains in the shear zone are highly oriented in the FD with the local symmetry axis slightly tilted inwards towards the core. This tilt angle tends to be the largest at the interior portions of the shear crystallized zone essentially following an approximate parabolic profile indicating that this feature of the structure is established by the spatial variation of the flow kinematics during injection. The microbeam X-ray pole figure results indicate that the *a*- and *b*-axes of the α crystals are distributed in a plane close to the ND–TD plane in the skin and shear zone. The level of orientation gradually decreases towards the mid symmetry plane at the interior of the samples from the slow cooling that takes place in these regions. The addition of small amount of diluent PMMA was found to enhance the chain orientation levels in the PVDF. This was attributed to the increase of melt viscosity as well as reduction of "self" entanglements of the crystallizable PVDF chains.

Keywords: Microbeam WAXS pole figure technique; SAXS technique; Structural hierarchy

1. Introduction

The injection molding process imposes complex thermal and stress effects on the injection molded parts. Moreover, the complex runner and mold geometries result in complicated flow patterns of the molten polymers. Thus, the resulting orientation distribution becomes rather complicated. Such a complex orientation distribution, in turn, results in anisotropic properties of the molded parts. To quantify such complex structures, microbeam probing techniques such as X-ray, IR, Raman can be used to map the spatial variation of structural features. The microbeam X-ray studies in this area are rather sparse, as the techniques to probe the local structure are not readily available with the exception of highly specialized synchrotron beam lines. The micro WAXS studies in this area include injection molding of poly aryl ether ketone [1–3], thermotropic liquid crystalline polymer [4], polyethylene naphthalate [5,6], syndiotactic polystyrene [7], and polypropylene [8]. These studies were concentrated on establishing the relationship between the processing conditions and the local symmetry axes (principal direction) as well as orientation development.

The purpose of this paper is to determine the effect of an amorphous (diluent) polymer on the structural behavior of crystallizable (poly(vinylidene fluoride) (PVDF)) polymer under very high thermal and deformation fields imposed by the injection molding process. This pair of polymers is also well known to be melt miscible.

The main issues that are of concern are the effect of composition on the development of crystallinity and crystalline orientation in the PVDF as well as development of

* Corresponding author. Tel.: +1-330-972-6865; fax: +1-330-258-2339.
E-mail address: cakmak@uakron.edu (M. Cakmak).

0032-3861/01/$ - see front matter
PII: S0032-3861(00)00769-2

Table 1
Compositions of the blends prepared

Blend	Concentration (PVDF/PMMA wt%)
PVDF/PMMA	100/0, 85/15, 70/30, 55/45

superstructural textures as represented by the lamellae orientation and their dimensions and spacings.

These results include qualitative representation of molecular orientation using matrixing microbeam wide angle X-ray diffraction patterns and small angle X-ray scattering (SAXS) techniques and quantitative representation of molecular orientation using the biaxial orientation factors of White and Cakmak [9]. The depth profiling of biaxial orientation factors were achieved using the pole figure data obtained through the microbeam wide angle X-ray pole figure experiments. Optical birefringence extinction measurements were also performed in order to determine the skin to core spatial variation of local symmetry axes in injection molded samples.

2. Experimental procedures

2.1. Materials

PVDF (Kynar 720) was provided by Atochem. Its number and weight average molecular weights measured using the GPC method in DMF solution are 113,000 and 863,000, respectively. Poly(methyl methacrylate) (PMMA S10-001) was received from Cyro Industries. The average molecular weight of PMMA measured via solution viscosity is 110,000. As-received as well as blended pellets were dried in a vacuum oven at 80°C for at least 12 h prior to their processing. Blends of PVDF with PMMA were prepared by melt blending of the two components using a 30 mm JSW intermeshing co-rotating twin screw extruder. The temperatures for seven zones on the extruder and the die were set to 196, 196, 198, 198, 198, 198, 198, and 200°C, respectively. The screw speed was kept constant at 90 rpm for all the blends prepared. Neat PVDF was also extruded through the twin-screw extruder in order to keep the thermo-mechanical history the same for all the samples to be studied. The concentrations of the blends are tabulated in Table 1.

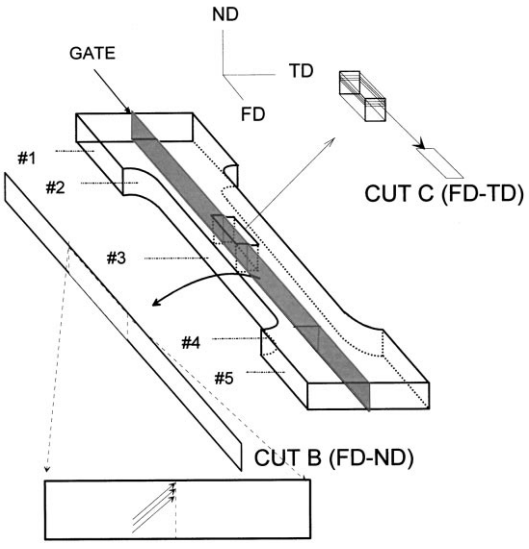

Fig. 1. Schematics of cutting procedures B and C.

The injection molding process was performed on a Boy (Model 15S) 15 ton reciprocating-screw injection molding machine equipped with a standard ASTM test mold and an oil circulating mold temperature controller. The temperature of the mold surface was measured using a pyrometer, and the injection speed was determined using a linear variable differential transformer (LVDT) that monitored the forward motion of the screw relative to the barrel. The samples were prepared at two different mold temperatures (40 and 120°C) and at two different injection speeds (with the average injection flow rates of 6.9 and 34.5 cm^3/s, respectively). The rest of the processing variables including barrel temperatures (195°C), injection pressure (13.8 MPa), back pressure (4.14 MPa), screw speed (165 rpm), and holding time (2 min) were kept constant. Large end-gated injection molded tensile bars were selected for all the analysis.

2.2. Sample sectioning

The samples for X-ray and optical birefringence extinction measurements were prepared using the cutting procedures B and C shown in Fig. 1. The cutting procedure B sections a thin ~0.3 mm slice along the mirror symmetry plane (FD–ND). This sample was used to take WAXS film patterns at a series of locations from skin to core with X-ray beam directed along the transverse direction (TD) indicated by arrows. This same sample was also used to determine the local symmetry axis direction through birefringence method. The samples that were cut with procedure C in FD–TD plane were used to take WAXS as well as SAXS film patterns with X-ray beam directed along the normal direction.

2.3. MicroWAXS pole figures

It is well known that the Injection molding process imparts very high spatial structural gradients in both non-crystallizable as well as crystallizable polymers. The literature on the non-crystallizable polymers is rather large as relatively easy optical techniques were used to characterize primarily birefringence profile [10–14] and on very rare occasions the local symmetry axes and their spatial variations [15]. In injection molded parts, it has been established that principal symmetry axes spatially varies in magnitude and direction with respect to the macro machine directions unlike some other melt processing operations such as melt spinning and tubular film blowing in which the principle

symmetry axes generally coincide with the macro machine directions (e.g. fiber axis along which the fiber is stretched, hoop and axial directions that form orthogonal axes in the tubular film blowing). These "macro" axes define the principal directions in the processed articles. In order to characterize the orientation behavior, both these spatially varying principal directions and the orientations with respect to these positions must be determined. For crystalline materials WAXS pole figure technique has been useful for quantitative determination of both of these properties. However, conventional pole figure devices use samples too large for adequate sampling of the sharp structural gradients that usually reside particularly near the surface layers of the parts. In order to study the quantitative variation of sharp structural gradients near the surface, we modified our Matrixing Micro beam X-ray diffraction camera to include rotation about one axis. In this case we chose ND direction as the rotation axis and probe the orientation gradient with a very small step size. The basic design of this apparatus is shown in Fig. 2.

2.3.1. Construction of microbeam X-ray pole figure

The microbeam X-ray pole figure technique that we developed is based on the flat plate photographic method. The construction of pole figures through photographic methods is not new and dates to early periods of crystallography when diffractometer methods were not available [16–19]. In this procedure, a crystalline sample is rotated about an experimental axis of the sample a number of steps. General geometry of the Micro beam pole figure system is shown in Fig. 2a and perspective view in Fig. 2b. In this design, we mounted a rotation stage on a precision X–Y translator. We chose the rotation (spindle) axis as the ND since the structural gradient in the mid plane of the injection molded sample is the steepest in the ND but not in FD and TD. As a result, the sample whose basal plane is very small $0.6 \times 0.6\ \text{mm}^2$ can be considered structurally invariant in FD and TD.

A series of X-ray patterns is taken at different rotational angles (γ) with the X-ray beam perpendicular to the axis of rotation using a microbeam X-ray camera. The azimuthal distribution of diffraction intensity of one particular reflecting plane (*hkl*) on the photographic film represents the azimuthal intensity distribution of the plane around the reflection circle as shown in Fig. 2c. This reflection circle is the intersection circle of the reciprocal lattice sphere of radius K/d_{hkl} and a sphere of radius K/λ with λ being the wavelength of the X-ray beam. Rotating the sample clockwise for an angle of γ with the X-ray beam fixed is equivalent to rotating the X-ray beam counter clockwise for an angle of γ with the sample orientation fixed. Therefore, the azimuthal intensity distribution on the photographic film after sample rotation with the X-ray beam in the direction of SO is the same as the azimuthal intensity distribution on the photographic film with the X-ray beam rotated to S′O with the sample orientation fixed. The new reflection circle after sample rotation (or X-ray beam rotation) is plotted as CD in Fig. 2c. By obtaining WAXS flat film patterns at a series of angles between $\gamma = 0^\circ$ and $\gamma = 180^\circ$ in a number of steps and digitizing the intensity distribution on each photographic film, a three dimensional intensity distribution of poles of (*hkl*) on the reciprocal lattice sphere can be determined. Such an intensity distribution forms the basis of the X-ray pole figure using the photographic method.

To generate a microbeam X-ray pole figure we need to first find the coordinate of each point on the reflection circles on the reciprocal lattice sphere. As shown in Fig. 2c, the center of the reciprocal lattice sphere is placed at the origin (point O) of the Cartesian coordinate (x, y, z).

The spindle axis of the specimen is located at S and is in parallel with the z-axis. We also establish another Cartesian coordinate (X, Y, Z) with its origin being coincident with the origin of the (x, y, z) coordinate and with its Z-axis being coincident with the z-axis of the (x, y, z) coordinate. The new reflection circle CD on the reciprocal lattice sphere after rotating the specimen clockwise for an angle of γ about its spindle axis is the intersection circle of the reciprocal lattice sphere and a cone with the cone angle being equal to $2(90 - \theta)$ (θ is the diffraction angle of the *hkl* plane) as shown in Fig. 2c. The cone tip (vertex) is located at the origin of the (X, Y, Z) coordinate and the symmetry axis of the cone is along the Y-axis in the (X, Y, Z) coordinate, which is obtained by rotating the (x, y, z) coordinate about the z-axis counter clockwise for an angle of γ.

The mathematical representation of the reflection circles in the (X, Y, Z) coordinate is shown in the following equations:

$$X = R \cos\theta \cos\delta \tag{1a}$$

$$Y = R \sin\theta \tag{1b}$$

$$Z = R \cos\theta \sin\delta \tag{1c}$$

where R is the radius of the reciprocal lattice sphere and δ the azimuthal angle of the reflection circle. The coordinate of each point on the new reflection circle CD or the rotated reflection circle in the (x, y, z) coordinate can be obtained through a coordinate transformation shown below

$$x = l_1X + l_2Y + l_3Z \tag{2a}$$

$$y = m_1X + m_2Y + m_3Z \tag{2b}$$

$$z = n_1X + n_2Y + n_3Z \tag{2c}$$

where l_i, m_i and n_i ($i = 1$, 2, and 3) are the directional cosines of the OX, OY, and OZ in the (x, y, z) coordinate. Since the X and Y axes make an angle γ with respect to the x and y axes, respectively, the above transformation becomes

$$x = X \cos\gamma - Y \sin\gamma \tag{3a}$$

$$y = X \sin\gamma + Y \cos\gamma \tag{3b}$$

$$z = Z \tag{3c}$$

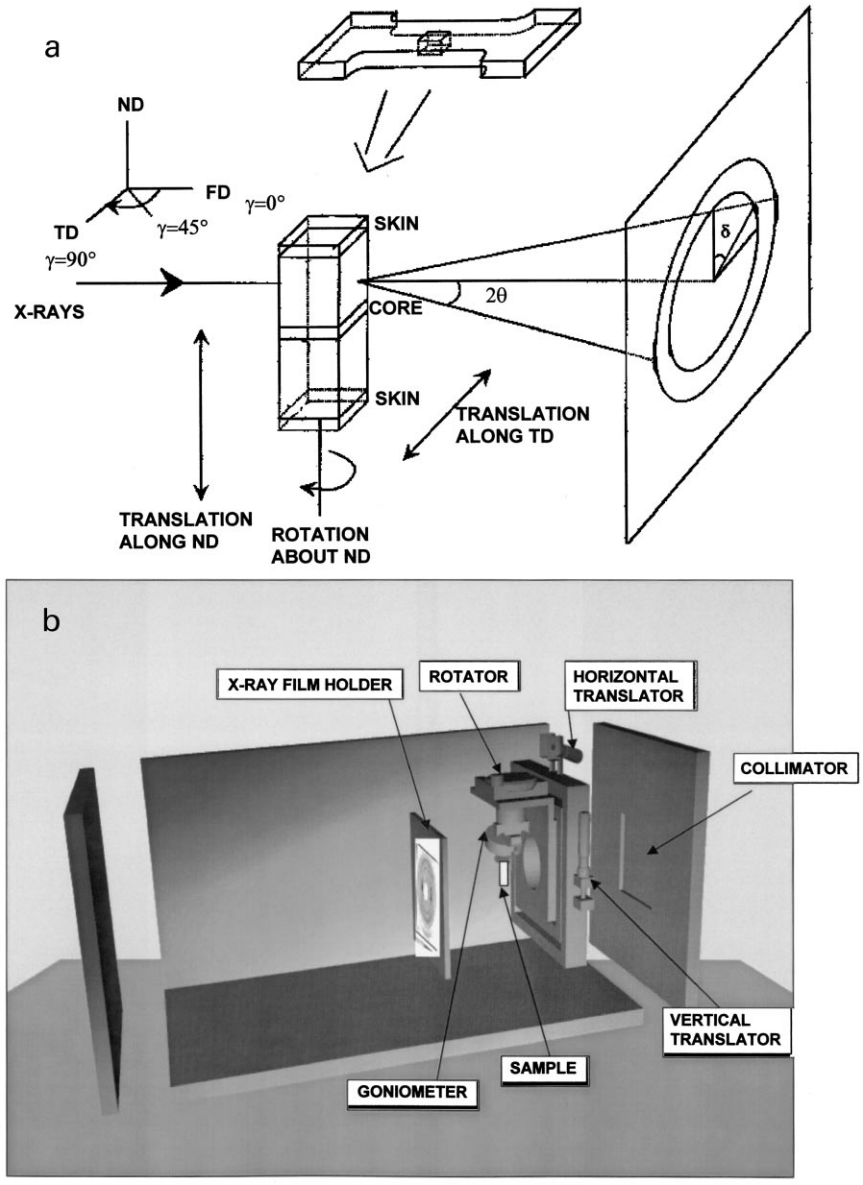

Fig. 2. (a) Schematic diagram of Microbeam WAXS pole figure system. (b) Microbeam pole figure camera and its components. (c) Reciprocal lattice sphere with incident beam SO and new reflection circle CD after sample rotation with new incident beam S′O. (d) Pole figure chart for (020) reflection of PVDF crystals in a Wulff net (equiangular projection).

Based on the above equations we can find the coordinate of each point on the rotated reflection circles in the reciprocal lattice sphere. If we project all the points on the reflection circles in the reciprocal lattice sphere to the *xz* plane using the equiangular projection method, we will obtain a pole figure projection in the Wulff net as shown in Fig. 2d. In this figure, the plus symbols represent the data points obtained in the actual pole figure plots. As it can be observed in this figure the complete sampling of the reciprocal space is not possible with flat plate diffraction geometry and a small zone is missing. However, this does not hinder the analysis as it will become apparent in the discussion of the data that the symmetry conditions that exist in the samples fill this gap.

2.4. Representation of molecular orientation

The quantitative description of orientation using an orientation factor was first introduced by Hermans and Platzek [20] for uniaxial orientation in fibers. Later Stein [21] introduced uniaxial orientation factors for different crystallographic axes.

To describe a more general state of orientation White and Spruiell [22–24] developed the biaxial orientation factors. These biaxial orientation factors have the following form:

$$f_1^{\mathrm{B}} = 2\,\overline{\cos^2\phi_1} + \overline{\cos^2\phi_2} - 1 \tag{4a}$$

$$f_2^{\mathrm{B}} = 2\,\overline{\cos^2\phi_2} + \overline{\cos^2\phi_1} - 1 \tag{4b}$$

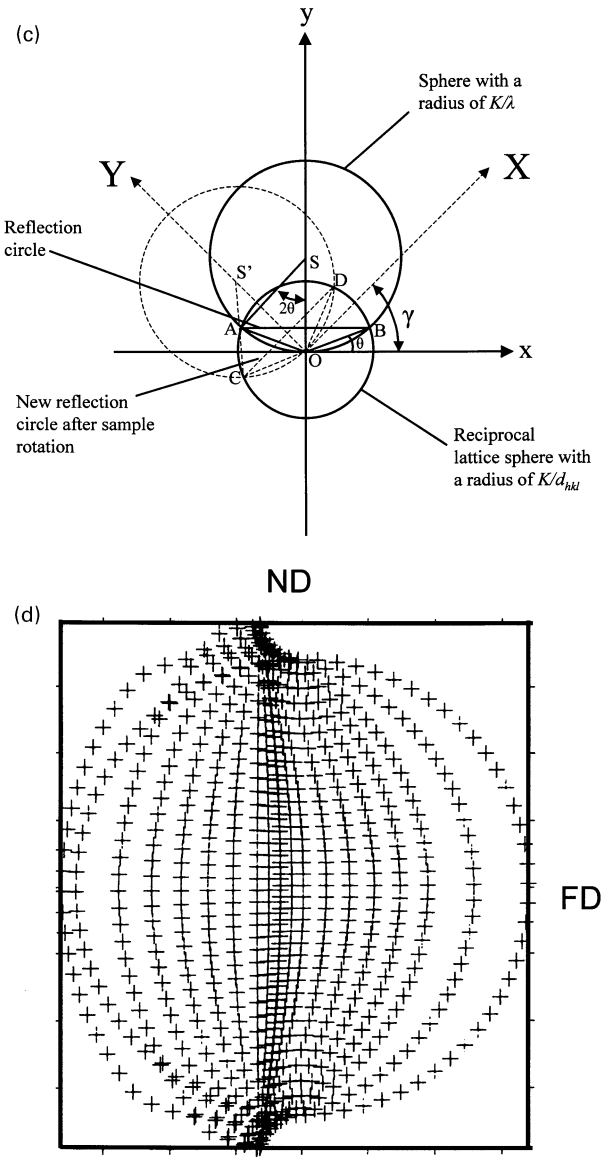

Fig. 2. (*continued*)

where 1, 2, and 3 represent the principal axes that are typically determined by the macro directions dictated by the processing machines (e.g. Machine, TDs). For a film, 1 and 2 directions can be in the plane of the film and 3 normal to the plane. ϕ_1 and ϕ_2 are angles between the crystallographic direction of interest, say, polymer chain axis and the 1 and 2 directions. In case of biaxially stretched films or tubular films, the principal axes generally coincide with the laboratory directions (machine direction, transverse (or hoop) direction and normal direction). However, for injection molded samples, such coincidence may not exist especially at locations away from the surfaces. As a result, two additional parameters that define the spatial orientation of the local symmetry axes must be defined together with the orientation factors with respect to these axes. This variability of local symmetry axis direction was taken into account in the biaxial orientation factors of White and Cakmak [9] to quantitatively describe the degree of orientation from skin to core of the injection molded sample.

In White and Cakmak's formulation [9], the orientation was expressed through the asymmetry of the polarizability tensor assuming the local symmetry directions differ from laboratory machine and TDs. Their formulation led to a set of biaxial orientation factors (equivalent to those of White and Spruiell) defined relative to the symmetry axes I, II, III and a set of angles ϑ_{I1}, ϑ_{II2}, ϑ_{III3} representing the directions of the axes relative to the laboratory axes (1, 2, 3) such as the machine or flow direction (FD) (1), transverse (2) and thickness (normal) (3) directions.

$$f_{\mathrm{I}}^{\mathrm{B}} = 2\,\overline{\cos^2\phi_{\mathrm{I}}} + \overline{\cos^2\phi_{\mathrm{II}}} - 1 \tag{5a}$$

$$f_{\mathrm{II}}^{\mathrm{B}} = 2\,\overline{\cos^2\phi_{\mathrm{II}}} + \overline{\cos^2\phi_{\mathrm{I}}} - 1 \tag{5b}$$

where I, II, III is the principal axis coordinate system which may differ from the laboratory (machine) directions. ϕ_{I} and ϕ_{II} are angles between the polymer chain axes and the I and II directions.

For crystalline polymers such as PVDF, we define the orientation factors for the crystallographic axes j

$$f_{\mathrm{I}j}^{\mathrm{B}} = 2\,\overline{\cos^2\phi_{\mathrm{I}j}} + \overline{\cos^2\phi_{\mathrm{II}j}} - 1 \tag{6a}$$

$$f_{\mathrm{II}j}^{\mathrm{B}} = 2\,\overline{\cos^2\phi_{\mathrm{II}j}} + \overline{\cos^2\phi_{\mathrm{I}j}} - 1 \tag{6b}$$

where j represents the a, b or c crystallographic axes.

2.5. Micro WAXS results

To study the orientation gradient from surface to core, the injection molded PVDF/PMMA samples were sliced in the FD–ND plane along the centerline of the sample using the cutting procedure B as shown in Fig. 1. The wide angle X-ray diffraction patterns were then obtained at a series of locations from surface to core with the X-ray beam perpendicular to the cutting plane using a matrixing microbeam camera [25,8] equipped with a precision x–y translation stage. This camera was mounted on a 12 kW Rigaku rotating anode generator operated at 40 kV and 150 mA. Nickel foil filter was used to obtain CuKα radiation. The X-ray beam size was about 100 μm.

In order to obtain the direction of local symmetry axis — quantified as the angle between the local symmetry axis and FD (tilt angle) — the WAXD patterns taken at different positions from skin to core were first digitized using a Sony 3 CCD video camera. The digitized images were then analyzed using an image analysis software on a Sun Workstation and the intensity profiles along the azimuthal direction for the $hk0$ planes of the PVDF α crystalline phase were obtained. The tilt angles of the intensity maxima along the azimuthal direction for the $hk0$ reflection planes were determined using a computer program and the tilt angles were taken as representatives of the local symmetry directions with respect to the FD. The tilt angles obtained

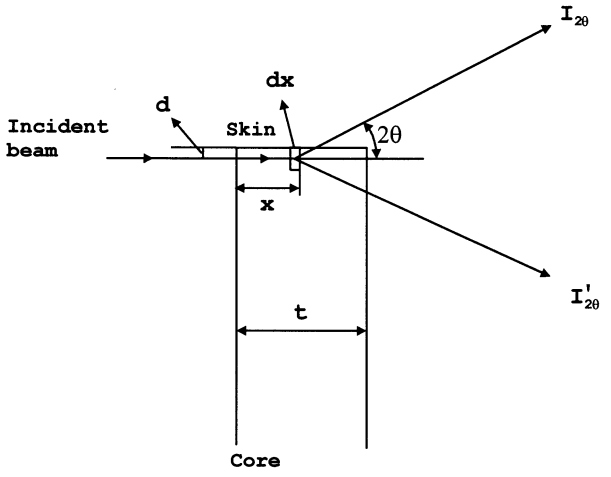

Fig. 3. Absorption difference due to the path difference of the diffracted beams.

using WAXD technique were also compared with the results obtained using the optical birefringence extinction measurements.

To further study the molecular orientation in the FD–TD plane, WAXS film patterns were taken from skin to core on C-cut slices of the PVDF sample molded at 40°C mold temperature and at 6.9 cm^3/s injection flow rate using the microbeam wide angle X-ray diffraction camera. The sliced samples were mounted on the camera with the X-ray beam oriented along the normal direction of the tensile bar. These diffraction patterns can provide statistical information on the molecular orientation distribution in the FD–TD plane.

2.6. Birefringence extinction measurements

To determine the local symmetry directions with respect to the macroscopic flow and normal directions, optical birefringence extinction measurements were performed on the samples cut along the centerline of the tensile bar using the cutting procedure B shown in Fig. 1.

In this procedure, the sample of about 300 μm thick is first placed on the cross polarized optical microscope (Leitz Labolux 12 Pol S) with the left skin parallel to the polarization direction of the polarizer. The sample is then rotated in order to find the angle where the transmitted light intensity becomes the lowest at a given depth from surface. This angle was taken as the birefringence extinction angle representing the local symmetry axis at that position. The same measurement was repeated at different positions from skin to core. This procedure assumes that one of the principal planes of the orientation distribution lies within this mirror symmetry plane thereby requiring the determination of one angle. Away from this mirror symmetry plane, the local symmetry axis may not be defined with one tilt angle but two as they may not coincide with the macro planes (FD–TD, FD–ND, TD–ND) as determined by geometry.

The birefringence extinction measurements were performed starting from both the left skin and the right skin of the sample. The extinction angles obtained from both sides of the sample at the same distance from the skin surface were averaged and the averaged results were plotted as a function of the distance from skin.

2.7. Microbeam wide angle X-ray pole figure

Fig. 2a and b shows the schematics and perspective views of the microbeam X-ray pole figure device we designed and built in our laboratory. The whole attachment was designed in such a way that it can be mounted onto our existing microbeam X-ray camera [25]. The specimen cut from the injection molded sample can be mounted on the sample mounting stage of the goniometer which is attached to a rotator. The rotator is mounted on a x–y translation stage, which provides the vertical and horizontal motions for the specimen.

To begin the experiment, the specimen was first cut at #3 position along the centerline (Fig. 2a) from the PVDF sample molded at 40°C mold temperature and at 6.9 cm^3/s injection flow rate. The spindle axis of the specimen was along the thickness direction of the molded sample. The cut specimen was then mounted onto the specimen mounting stage of the goniometer, and the position and the alignment of the specimen was adjusted by adjusting the x–y stage and the goniometer. This procedure was performed on a laser beam alignment system built in our laboratory in order to align and position the specimen in such a way that the X-ray beam hits the specimen in a proper position. The precise positioning of the specimen was performed by taking a series of X-ray patterns at different x, y positions and finding the edges of the specimen.

Once the position (specific distance from the surface of the sample) of the sample was fixed, a series of X-ray patterns was taken at that particular position at different angles by rotating the specimen stepwise. Since the specimen was cut from the centerline of the tensile bar, there exists a mirror symmetry plane along the FD–ND plane. A series of rotations from $\gamma = 0$ to 90° was enough to generate a full pole figure based on this symmetry assumption. The obtained diffraction patterns were then digitized using a 16 bit Photometrics CCD camera after a routine intensity calibration procedure. The azimuthal intensity distributions for the strong reflection planes (110) and (020) of the α crystalline form were used to build the microbeam X-ray pole figures using the transformation procedure described in the previous section.

2.7.1. Absorption correction

Unlike most other polymers, PVDF strongly absorbs X-rays. When X-ray hits the skin part of the specimen, the diffracted beam $I_{2\theta}$ and $I'_{2\theta}$ travel through different paths of different lengths as shown in Fig. 3. The path of shorter length gives higher diffraction intensity at the upper quadrant of the WAXS pattern due to the lower level of

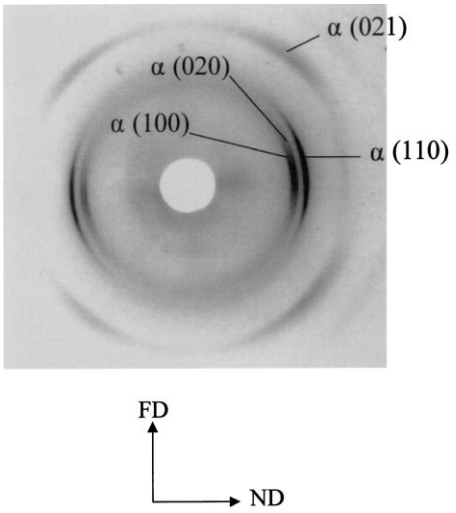

Fig. 4. Typical WAXD pattern obtained in the shear region of the PVDF sample molded at 6.9 cc/s injection speed and at 40°C mold temperature.

absorption. As a result, we may see non symmetric azimuthal intensity distribution at positions closer to skin at $\gamma = 0$ due to the difference in the absorption.

To compensate for the absorption difference we performed an absorption correction for all the X-ray patterns obtained at positions closer to the skin. We first calculated the linear absorption coefficient for PVDF using a standard procedure [26]. The following linear absorption coefficients were obtained:

Crystalline (α): 22.02 cm^{-1}.
Amorphous: 19.27 cm^{-1}.
Semicrystalline PVDF (55% crystallinity): 20.79 cm^{-1}.

In Fig. 3, we assume that the direct X-ray beam enters the specimen of thickness t. Let I_o be the intensity diffracted by unit volume of the specimen at 2θ angle assuming no absorption. We then have the intensity diffracted at 2θ by the volume $A\,dx$

$$dI_{2\theta} = I_0 A \exp\left(-\mu\left(x + \frac{d}{\sin 2\theta}\right)\right)dx \tag{7}$$

$$I_{2\theta} = I_0 A \frac{1}{\mu}\left(\exp^{-\mu(d/\sin 2\theta)} - \exp^{-\mu(t+(d/\sin 2\theta))}\right) \tag{8}$$

where d is the distance between X-ray beam and the surface of the specimen (skin). It is important to note that the above equations can only be used when d is small enough compared to the thickness of the sample t since the path length changes when x approaches the value of t. The azimuthal intensity of the film from $\delta = 0$ to 180° can be corrected using the above equations neglecting the path change of the diffracted ray at different azimuthal angles from $\delta = 0$ to 180°. Similarly, we also have at the other half of the specimen

$$dI'_{2\theta} = I_0 A \exp\left(-\mu\left(x + \frac{t-x}{\cos 2\theta}\right)\right)dx \tag{9}$$

$$I'_{2\theta} = \frac{I_0 A}{\mu(1 - \sec 2\theta)}\exp(-\mu t \sec 2\theta) \times\{1 - \exp[-\mu t(1 - \sec 2\theta)]\} \tag{10}$$

In our experiment, the azimuthal intensity was corrected for each film using Eqs. (8) and (10) with μ being the linear absorption coefficient of semicrystalline PVDF (55% crystallinity for the PVDF sample tested). I_0 was obtained and subtracted by a constant intensity value (amorphous background) for each azimuthal angle. The background corrected intensity data were then used in our microbeam X-ray pole figure plot and orientation factor calculations.

2.8. SAXS

SAXS studies on injection molded PVDF/PMMA samples were performed on a GE X-ray generator (operated at 30 kV and 30 mA) equipped with a Furnas X-ray camera. Nickel foil filter was used to obtain CuKα radiation and vacuum was applied to the camera to reduce the air scattering. The sample to film distance was 50.25 cm. The typical exposure time was about 3 h.

The long spacing (L) of the lamellae at different positions from skin to core were calculated from the scattering angle (θ^0) where we observe the maximum scattering intensity using the following equation:

$$2L \sin \theta^0 = n\lambda \tag{11}$$

where λ is the wavelength of the X-ray which is 1.5418 Å.

The lamellar thickness (d_{cry}) was also calculated from the long spacing using the following equation assuming a two-phase model provided that the crystallinity (X) is known from the DSC measurements.

$$d_{cry} = LX \tag{12a}$$

$$d_{am} = L(1 - X) \tag{12b}$$

3. Results and discussion

3.1. Wide angle X-ray diffraction

3.1.1. Injection molded PVDF samples

Fig. 4 shows a diffraction pattern obtained in the shear region of the sample molded at 40°C mold temperature and at 6.9 cm^3/s injection flow rate. This pattern represents a typical diffraction pattern of the α crystalline form. Among all the diffraction peaks, (100), (020) and (110) planes of the α form (form II) are the strongest and a weaker (021) peak in the first layer line is observable. In our studies

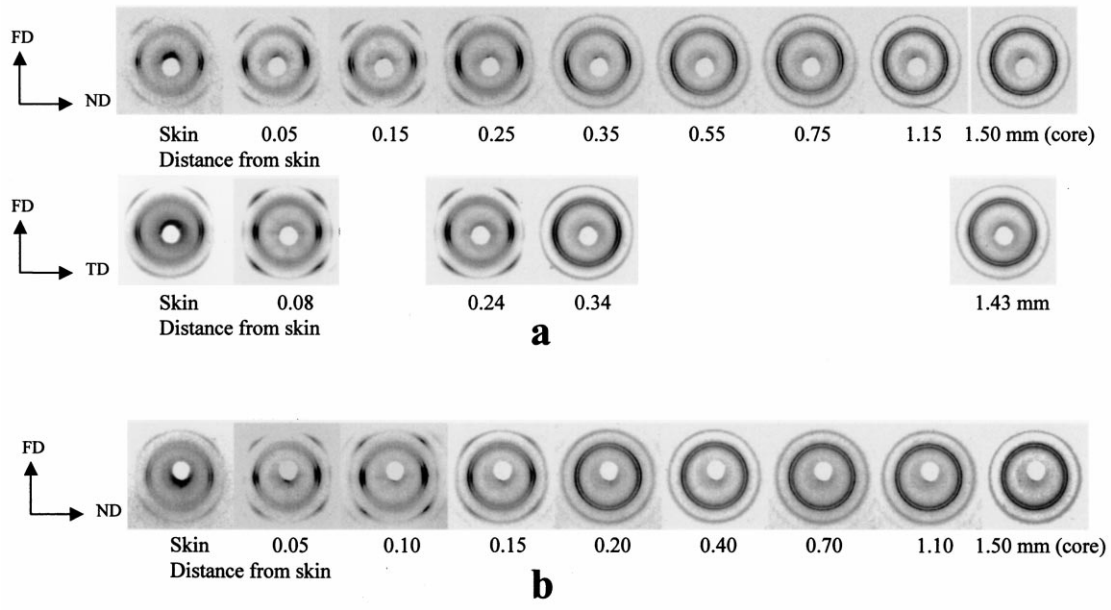

Fig. 5. Micro WAXS patterns obtained from skin to core on 100/0 (PVDF/PMMA) samples processed at 6.9 cc/s injection speed (a) 40°C mold temperature; (b) 120°C mold temperature.

presented below, we did not detect crystalline peaks corresponding to β form (form I) or other crystalline forms.

Fig. 5a shows the micro-WAXD patterns taken at different locations from skin to core for PVDF sample (B cut) molded at 40°C with an average injection flow rate of 6.9 cm^3/s. Three distinct regions can be distinguished. About 50 μm thickness of the surface layer, was formed as a result of the extensional flow at the flow front. The chain axes in this layer are highly oriented in the FD as indicated by the diffraction arcs from (100), (020) and (110) planes concentrated along the equatorial direction. In this orientation the equatorial direction corresponds to ND. The second pattern at 0.05 mm represents the transition region from the skin to the shear zone. It should be pointed out that there is a significant tilting of the local symmetry axis towards the core as evidenced by the rotation of the symmetry axis of the pattern towards the right (towards the core). The shear zone is about 0.2 mm thick in this case. The molecular chains in this layer are highly oriented and the local symmetry axes are tilted towards the core. This tilting phenomenon in the shear zone has also been observed in the injection molded thermotropic liquid crystalline polymers [4], poly(aryl ether ketone) [2], polypropylene [27], and polyethylene [28]. It is a manifestation of the parabolic nature of the flow field that took place during the injection stage. The observation of this tilt signifies that the orientation profile developed in this "flow field" remains largely in tact during the holding stage where the material crystallized under a time varying temperature gradient. Towards the core, we observe the azimuthal broadening of the diffraction arcs due to decreased levels of orientation and the local symmetry axis seems to be further tilted towards the core. At this point we begin to see the spherulites under the cross polarizers using the polarizing microscope [29]. However, the WAXS patterns at the core still exhibits azimuthal intensity distribution. This clearly suggests that the unoriented "component" of the structure co-exists with the "oriented" shish or shish kebabs.

The WAXS patterns taken on the samples that were cut in the FD–TD plane (C-cut) exhibit similar azimuthal intensity profiles to the B-cut samples shown in the first row particularly near the surface. However, slightly increased intensities of (110), (020), and (100) planes in the meridional direction in these regions suggest the presence of certain level of chain axis orientation towards the TD in the skin and shear zone. This is not entirely unusual as the biaxial deformation field at the flow front is expected to cause this orientation behavior particularly away from the mid-symmetry plane (FD–ND) towards the corners of the cross-section. However, despite this variation, locally, these regions exhibit symmetry close to transverse isotropy. Quantitative characterization of the *c*-axis orientation using the microbeam X-ray pole figure technique will be given in the later sections.

One of the manifestations of the tilting of the symmetry axis can be observed in the C-cut sample at 0.34 mm depth from the surface. The intensities of the (021) peaks in the upper quadrants are slightly lower than the lower quadrants. This is a typical data if one were to take a WAXS pattern of a fiber that is tilted towards the X-ray beam (see for example Alexander [26] p. 201 showing a similar example).

As shown in Fig. 5b, the increase of mold temperature to 120°C causes a reduction of thickness of the skin layer and the shear zone as these "highly oriented" regions concentrate closer to the surface. In parallel with the above behavior, the symmetry axes do not deviate from the FD

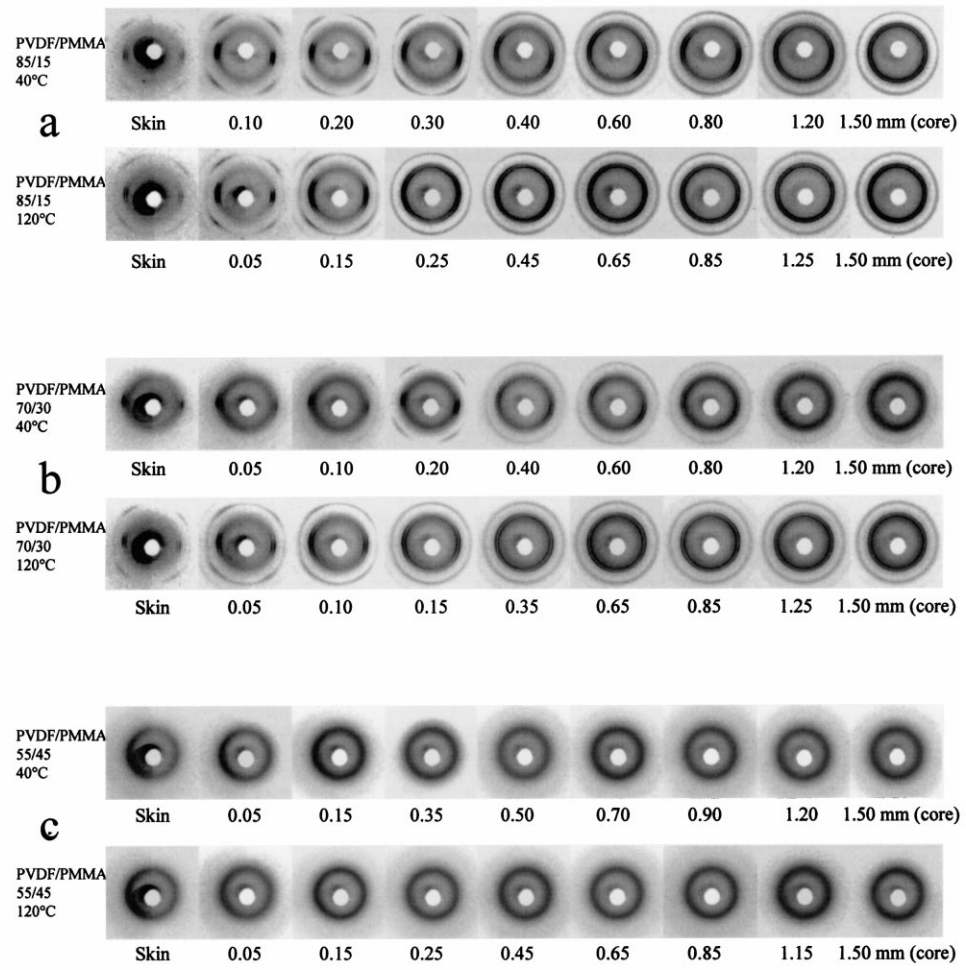

Fig. 6. Micro WAXS patterns obtained from skin to core in: (a) 85/15; (b) 70/30; and (c) 55/45 samples molded at 6.9 cc/s injection speed and at 40 and 120°C mold temperatures.

significantly. Since the injection speed was kept the same, the main mechanism controlling this structural formation is the temperature difference between the melt and mold temperature as it directly controls the local temperature gradient and the speed of solidification front during the injection.

The "diffuse" inner boundary between the shear zone and core is defined as the location of the solidification front when the flow stops at the end of the injection stage. This "local" structural formation mechanism does not explain the orientation behavior observed further inward towards the core. This, we strongly believe, is a result of the formation of the oriented crystallites upstream as highly oriented and crystalline "threads" that are transported down stream where they are observed to be mixed with the "apparently" unoriented spherulitic texture. We will revisit this hypothesis at the structural model section in the companion paper where light scattering results will be presented [30].

3.1.2. Injection molded blends of PVDF with PMMA

Addition of 15% PMMA does not change the overall orientation behavior of the samples as shown in Fig. 6a for 40 and 120°C mold temperatures. The strong crystalline reflections exhibited by the sample (110), (020), and (100) planes belong to the α form. The low mold temperature results in the formation of thick oriented layers near the surface and local symmetry axis tilts towards the core following the "imprint" of the local flow kinematic profile that took place during filling.

When we further increase the PMMA content to 30 wt%, the WAXS patterns become weak and diffuse as shown in Fig. 6b. This is primarily due to the decreased level of crystallizability in this composition. However, the effect of flow on the diffraction patterns is still quite significant. The position of the diffraction arcs from (110), (020), and (100) planes of the α crystalline form in the skin and shear zone indicates that the chains in these regions are highly oriented and the usual local tilt towards the core is present at 40°C mold temperature. A closer inspection of these WAXS patterns reveals that the azimuthal spread of the visible equatorial crystalline diffraction peaks are much narrower than those observed in the samples containing smaller amounts of PMMA (15 wt%). This fact clearly

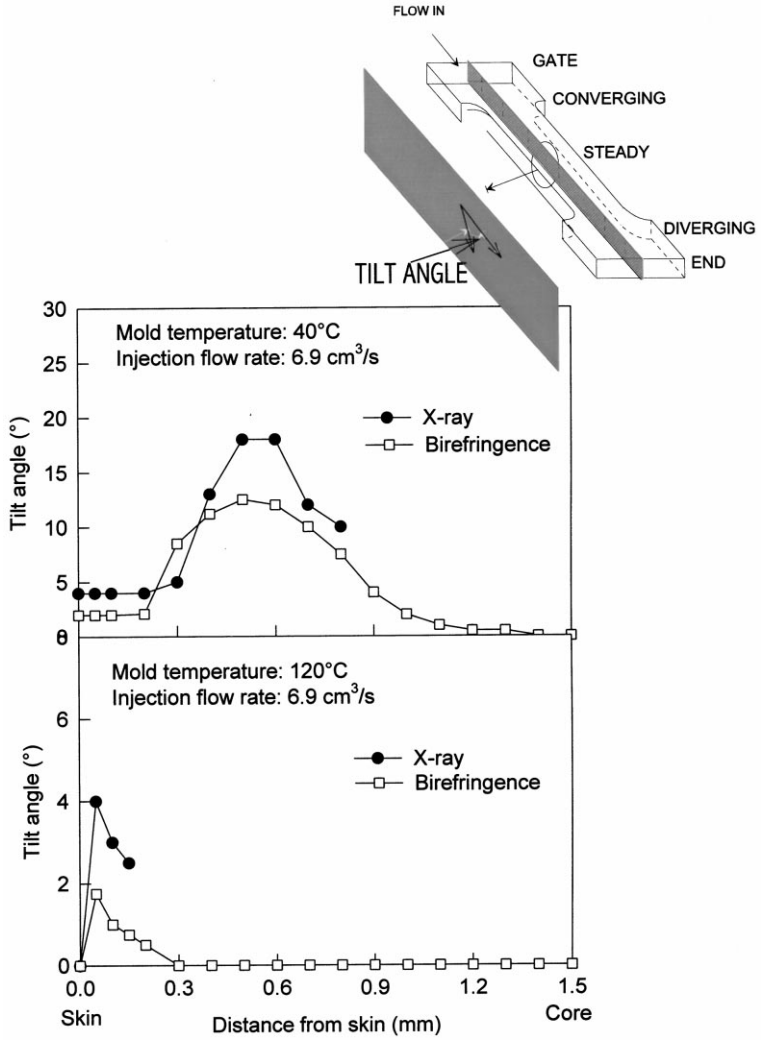

Fig. 7. Tilt angle versus distance from skin (at #3 position) for PVDF samples molded at 40 and 120°C mold temperatures (6.9 cm^3/s injection flow rate).

suggests that the addition of more non-crystallizable PMMA diluent results in the increased levels of crystalline chain orientation near the surfaces of the samples as compared to 85% PVDF samples. This could be attributed to the increased environmental stiffening that is experienced by the crystallizable PVDF chains in the presence of stiffer PMMA chains resulting in preservation of larger portion of orientation developed during the flow as the relaxation process is greatly reduced. The interior of these samples essentially shows no crystalline forms deeper than 0.8 mm. It should be emphasized that if the thermally activated crystallization were to play a role in these regions the opposite highly crystalline structure in the core should have occurred since the chains in the interior experience much lower cooling rates as compared to the skin. This demonstrates that all the crystallization that is observed near the skin is exclusively caused by the orientation induced crystallization.

At 55/45 PVDF/PMMA composition, the ability to crystallize is lost under the processing conditions used in this research. The samples neither show any flow induced crystallization near the surface nor thermally induced crystallization in the core. All WAXS patterns exhibit an amorphous halo. This confirms our previous crystallinity observations obtained from the DSC measurements published earlier [29].

3.2. Determination of the local symmetry directions

3.2.1. Injection molded PVDF samples

As indicated earlier, the local symmetry axes deviate away from the FD towards the core at positions away from the surface. In order to quantify these changes, we determined this angle ($= 0°$ when the symmetry axis coincides with the FD) from the azimuthal intensity profile of the (110) plane of the α form on the WAXD patterns obtained from the B-cut samples shown in Fig. 5. This measurement was also verified by the optical extinction method described earlier.

Fig. 7 shows the tilt angle vs. the distance from skin for

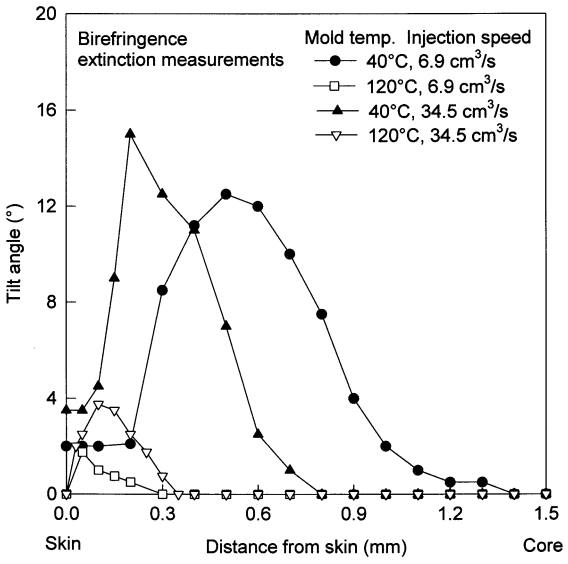

Fig. 8. Tilt angle versus distance from skin (at #3 position) for PVDF samples molded under different conditions.

the PVDF samples molded at 40 and 120°C mold temperatures. The tilt angles determined using WAXD patterns and the optical technique are quantitatively quite comparable.

At 40°C mold temperature, the tilt angle remains constant near the skin at very small values of 2–4° practically in alignment with the FD. Beyond this level the angle increases to a maximum value of 15–20° before diminishing towards the core. In the core, the chain tilting phenomenon is almost absent since orientation decreases significantly.

As indicated earlier, this tilt angle profile resembles the parabolic flow profile of the material during the injection molding process. In the skin and shear zone the molecular orientation is frozen in due to the fairly fast cooling rate. Towards the core, the orientation and local symmetry profile are extensively changed as the chains oriented during flow are increasingly able to relax after the cessation of flow due to the reduction of cooling rates experienced by the material.

As qualitatively observed in Fig. 5, the tilt angle at the high mold temperature peaks at positions closer to the skin and their magnitude is much smaller than those observed at the low mold temperature. This reflects the fundamental differences in the thermal deformation behavior experienced by the chains as the mold temperature is increased.

3.2.2. Effect of mold temperature and injection speed

The influence of injection flow rate on the tilt angle profile at two mold temperatures is shown in Fig. 8. With increasing injection speed, It was not surprising to observe the movement of the maximum tilt angle position towards the surface as it is demonstrated at 40°C mold temperature. However, it was rather surprising to observe that the magnitude of the peak was actually higher when the higher injection speed was employed. At the low mold temperature the sample that was injected faster reaches the peak value closer to the surface and the peak decays away at a position closer to the surface. This could be explained with a perspective on the dynamic progress of the frozen front during the injection process. The samples molded at the lower mold temperature (40°C) show much larger tilt angle maxima and the positions of the maxima are farther away from the skin compared to the samples molded at the higher mold temperature (120°C). The tilt angle profiles are directly related to the thickness of the skin and shear layers formed during the injection stage. The thinner the skin and shear layers (for example, at the higher mold temperature), the closer the tilt angle maximum is to the skin.

3.2.3. Injection molded blends of PVDF with PMMA

The effect of the addition of PMMA on the tilt angle from skin to core for the injection molded blends of PVDF with PMMA can be seen from Fig. 9. The broadest distribution of the tilt angles is observed in the samples molded at the low injection speed with the low mold temperature. This is expected as the frozen layer advances much deeper into the core regions at low injection speeds during the filling. As a result, the zone of influence of the solid–liquid boundary sweep at a given position is more substantial under such conditions. The increase in injection speed narrows this distribution and moves the peak positions towards the sample surface. These observations suggest that the local symmetry axis direction is influenced mostly

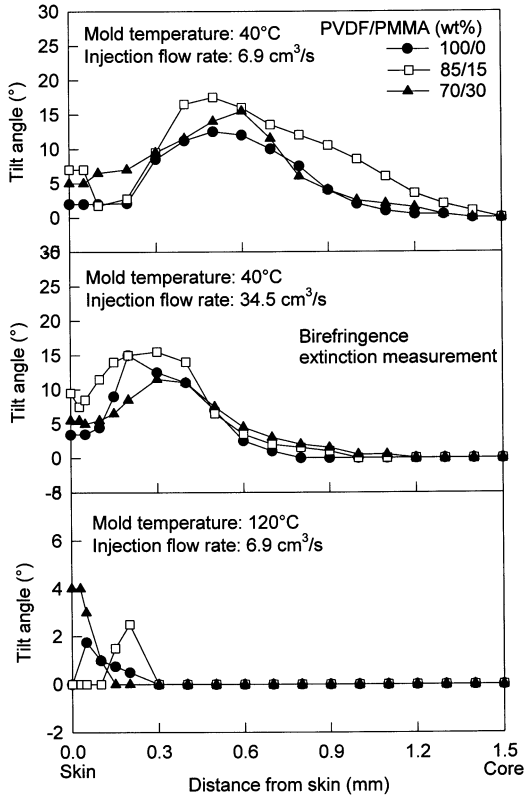

Fig. 9. Tilt angle versus distance from skin (at #3 position) for PVDF/PMMA blends molded under different conditions.

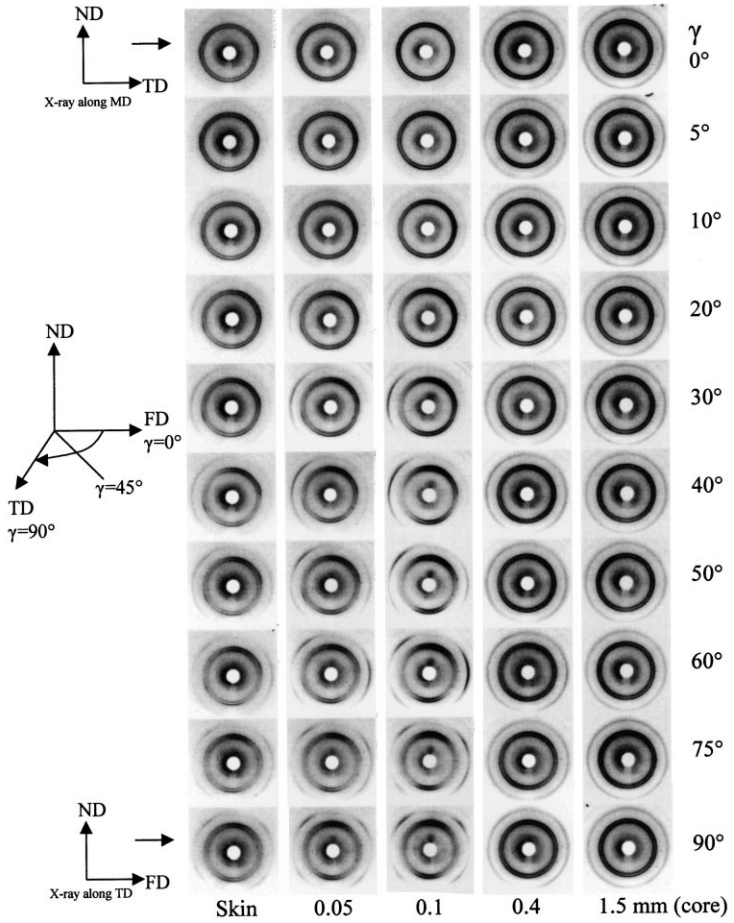

Fig. 10. Microbeam X-ray pole figure rotational experimental procedure. WAXS patterns are obtained with PVDF sample molded at 40°C mold temperature and at 6.9 cc/s injection flow rate.

by the changes in the mold temperature. In common with this behavior is the development of the frozen layer thickness during the injection stage as both the injection speed and mold temperature can control this process thereby resulting in similar effects.

3.3. Microbeam X-ray pole figure

Fig. 10 shows the Micro WAXS film patterns obtained using microbeam pole figure system, at a series of γ rotation angles about the ND axis. In this figure five sets of data are shown representing data obtained at five different locations from skin to core. The azimuthal intensity distribution obtained from (110) and (020) peaks were reconstructed on pole figures showing iso intensity contour plots as well as three dimensional intensity profiles for better viewing. In the construction of these pole figures, normal projection procedure was employed. In these pole figures (Figs. 11 and 12) the vertical direction is Normal direction (normal to the wide surface of the injection molded sample). The center of the pole figure represents the TD and horizontal direction represents the FD.

At the skin and the shear zone, the chains are highly oriented in the FD with a slight tilt towards the core. This tilting occurs in FD–ND plane confirming that the FD–ND mid-plane in these samples truly represents structural mirror symmetry plane. This also validates the earlier "single tilt angle" measurements that were made on the micro WAXS film patterns taken on B-cut samples with X-ray beam in the TD.

The (020) and (110) plane normals shown in the pole figures are fairly evenly distributed in a plane very close to the ND–TD plane. The intensities of the (110) planes are slightly higher in the Normal direction. The (020) peaks also exhibit slightly higher concentration of intensities in the ND as well as in the TD directions as evidenced by the appearance of peaks in these directions.

At about 0.1 mm from the sample surface, we observed maximum level of chain orientation among all the positions tested. This indicates that the highest crystalline orientation does not occur at the skin but approximately in the middle of the shear crystallized region. As we move towards the core, the level of chain orientation is greatly reduced. In the core (middle of the specimen, 1.5 mm from skin), the chains are randomly oriented as evidenced by the relatively flat intensity profiles of the (110) and (020) plane normals.

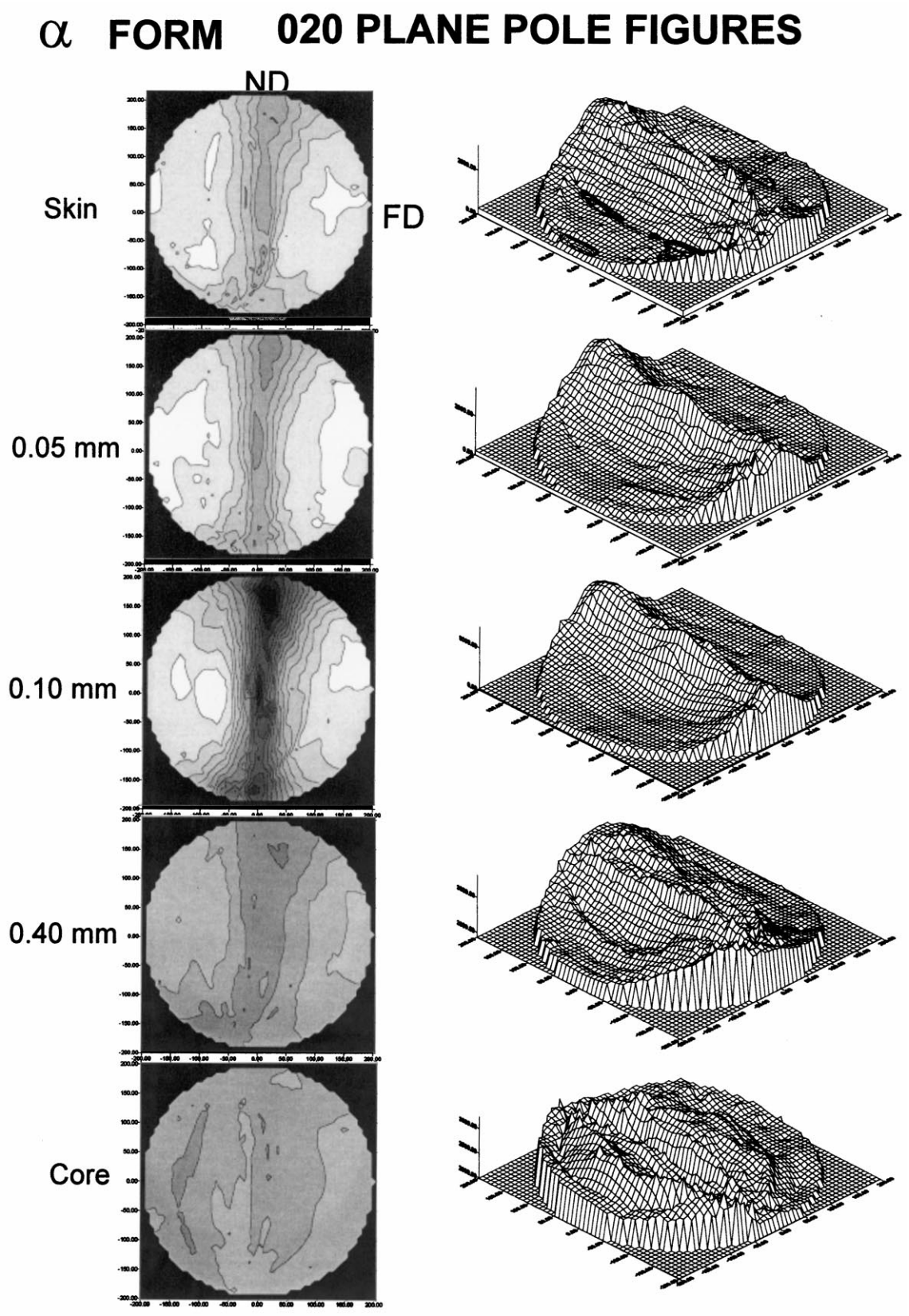

Fig. 11. Equiangular projection of pole figure (020 plane of α-crystalline form) at different positions from skin to core for PVDF sample molded at 40°C mold temperature and at 6.9 cm^3/s injection flow rate.

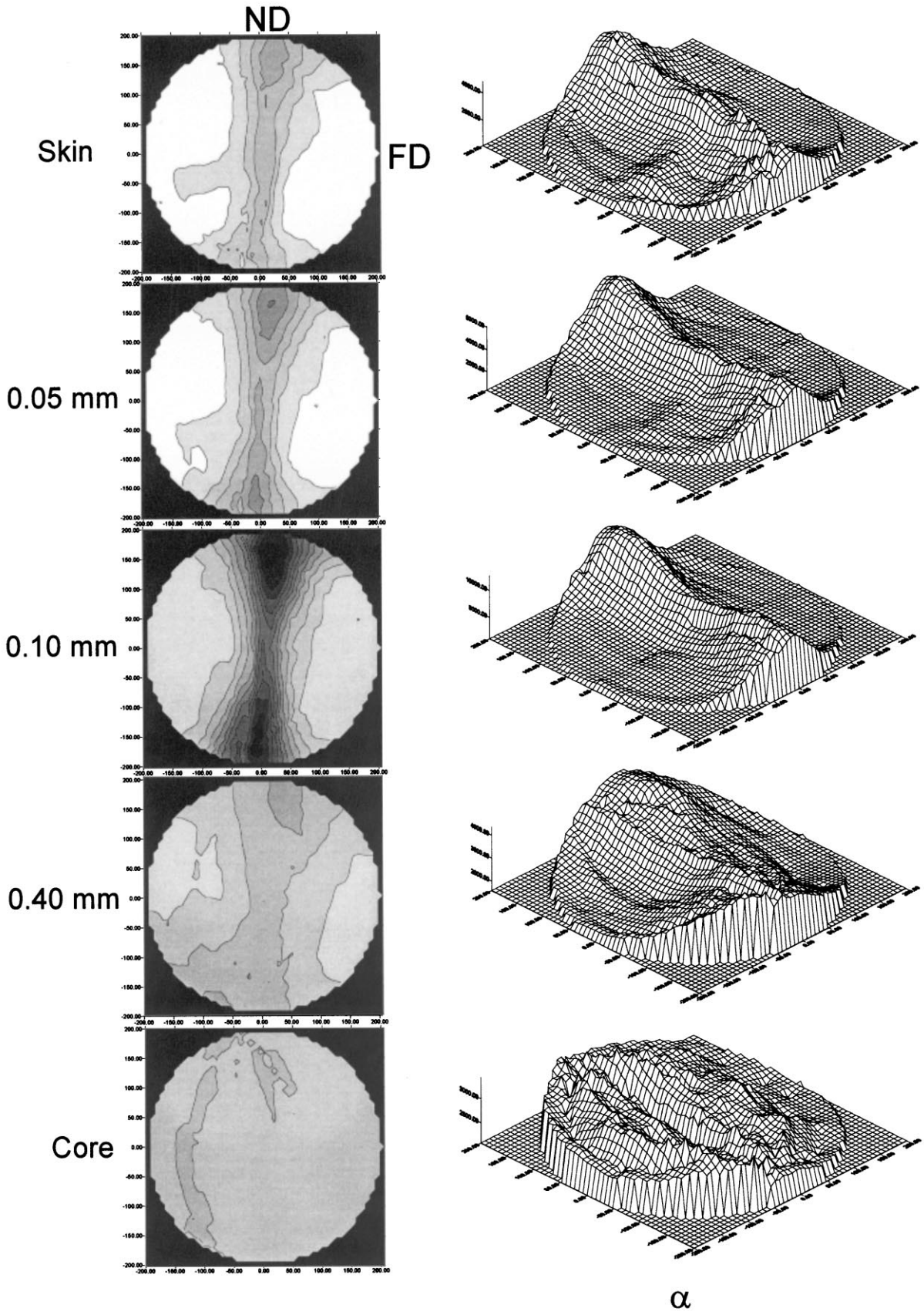

Fig. 12. Equiangular projection of pole figure (110 plane of α-crystalline form) at different positions from skin to core for PVDF sample molded at 40°C mold temperature and at 6.9 cm^3/s injection flow rate.

To evaluate the level of molecular orientation, we calculated the White and Cakmak's biaxial orientation factors using these microbeam X-ray pole figure data. The reciprocal lattice sphere was first numerically rotated for each set of pole figure data so that the principle axes of the sphere coincide with the local symmetry axes. The rotation angle was obtained at each position from skin to core from the X-ray tilt angle measurements described in the previous section. $\langle\cos^2\phi_{I,c}\rangle$ was determined for PVDF α crystalline phase using the following equation derived based on the Wilchinsky's rule [31,32].

$$\langle\cos^2\phi_{I,c}\rangle = 1 - 1.2647\langle\cos^2\phi_{I,110}\rangle - 0.7353\langle\cos^2\phi_{I,020}\rangle \quad (13)$$

Since the tilt angle as well as the two biaxial orientation factors need to be presented for each position, we chose to plot them in two different ways. Fig. 13a shows the three parameters as a function of position in the thickness direction in two different graphs. In the second method shown in Fig. 13b, only the biaxial orientation factors are presented without their local tilt angle on isosceles triangle whose vertexes represent the maximum orientation values in relation to the major symmetry axes.

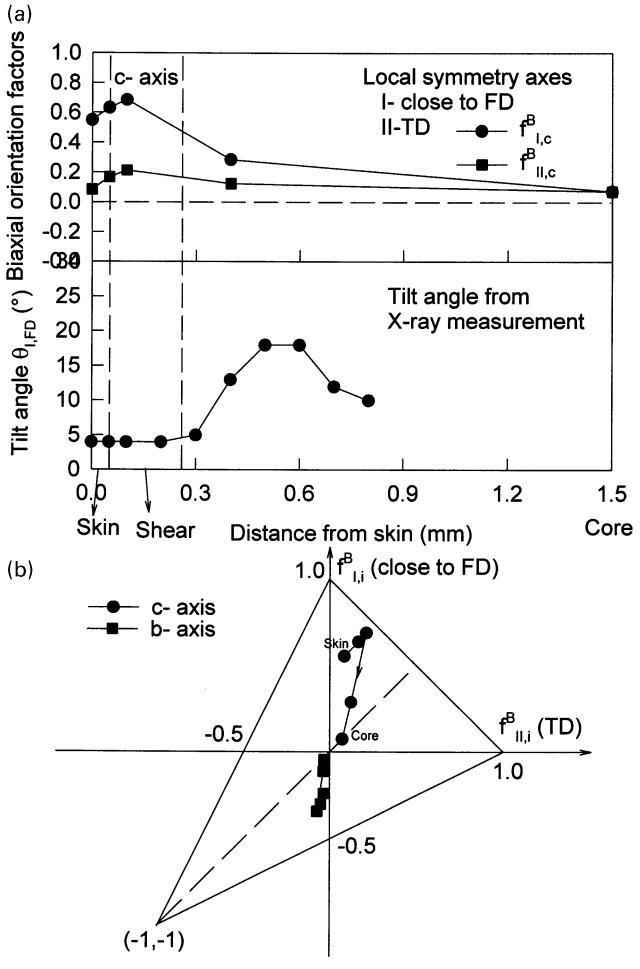

Fig. 13. Distributions of biaxial orientation factors for PVDF sample molded at 40°C mold temperature and at 6.9 cm^3/s injection flow rate (at #3 position along the center line).

Fig. 13a shows the *c*-axis biaxial orientation factors as a function of distance from skin for the PVDF sample molded at 40°C mold temperature and at 6.9 cm^3/s injection flow rate. It can be seen from this figure that the *c*-axis orientation along the local symmetry axis (close to FD) increases first and reaches a maximum level at 0.1 mm from the sample surface, and then decreases as the distance from skin increases. The two biaxial orientation factors are not equal to each other and the overall texture of the material is closer to being uniaxial in FD than equal biaxial. In the core (middle of the specimen, 1.5 mm from skin), the chains are almost randomly oriented. From Fig. 13 we can also see that there exists a very low degree of *c*-axis orientation along the TD in the skin and shear zone. The *b*-axis biaxial orientation factor along the "I" direction is negative indicating that *b*-axis is perpendicular to this direction (close to FD).

In summary, somewhat counter intuitively, the highest orientation levels are not found at the surface layers but somewhere in the middle of shear zone. The tilt angle remains constant and very small until one reaches the inner "diffuse" boundary of the shear region that was defined at the cessation of the flow. However, the orientation levels continue to persist even beyond this diffuse boundary while the tilt angle sharply increases following the contours of the flow field. This observation is contrary to the commonly perceived behavior. That is, the interiors of the samples are unoriented. In fact as Fig. 13a indicates the orientation levels persists well into the so-called core regions suggesting that there is an additional fundamental structural mechanism that is responsible for this preferential orientation of chains. We will further elaborate on this in the structural model section below.

3.4. SAXS

3.4.1. Injection molded PVDF samples

The SAXS pattern variation with distance from skin for PVDF samples molded at 40 and 120°C mold temperatures with 6.9 cm^3/s injection flow rate is shown in Fig. 14a and b, respectively.

At 40°C mold temperature, three distinct structural regions can be distinguished across the thickness. The first layer is the skin layer with a two-point discrete scattering pattern. The primary modulated crystalline–amorphous alternating structure is oriented in the FD. The fact that the 2-point pattern has a rather narrow distribution in the meridional direction suggests that the crystallization has taken place at a fairly narrow range at the skin, presumably under very rapid cooling of the biaxially stretched melt front upon contact with the mold surface. The second layer is the shear zone where we also observe the discrete meridional pattern. However, the shape of these two point discrete patterns changes to "tear-drop" in appearance. The tip of

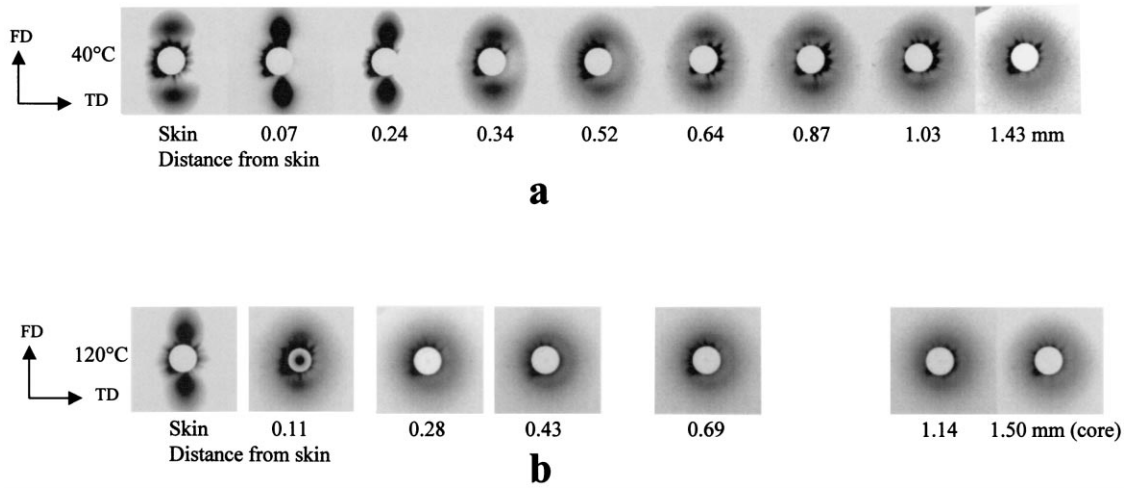

Fig. 14. SAXS patterns taken on microtomed thin slices(C cut) from skin to core for PVDF sample molded at 6.9 cm^3/s injection speed and at: (a) 40°C mold temperature; and (b) 120°C mold temperature.

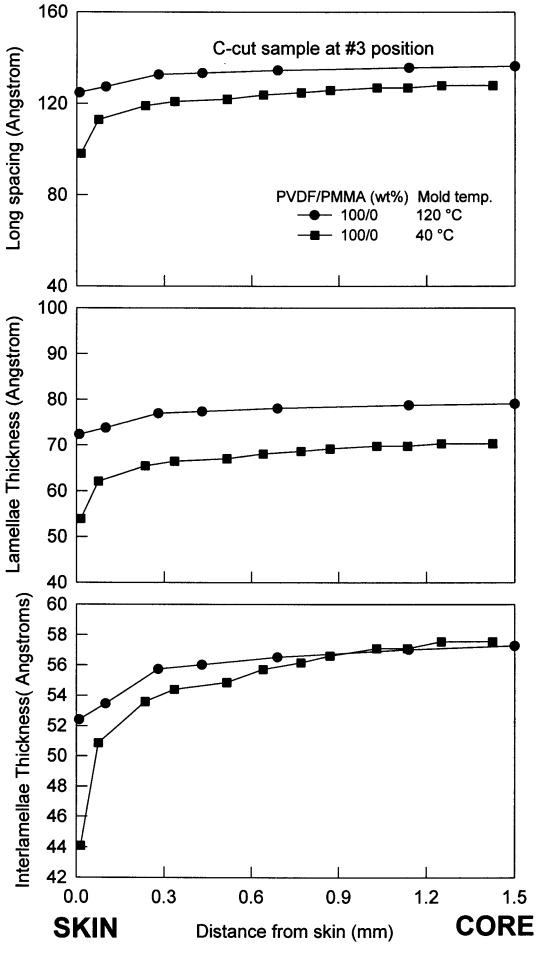

Fig. 15. Long spacing, lamellae and interlamellae thicknesses as a function of distance from skin for injection molded PVDF with an injection flow rate of 6.9 cm^3/s.

the pattern points towards the beam stop. One way to interpret this "tear-drop" pattern is by the detailed time evolution of "shish–kebab" structure. The "shish" regions have a distribution of long spacing resulting in intensity spread along the meridional direction. This is mainly caused by their crystallization at elevated temperatures under the influence of flow (resulting in larger long spacing). It is also suspected that these regions may be primarily formed by longer chains that are more susceptible to orienting effects of the flow and are known to have very long orientation relaxation times. This makes them easy to orient and once they are oriented they are difficult to randomize.

The reason there is considerable meridional variation in intensity may be due to multi stage structural formation process suggesting that in these regions the crystallization occurs over a span of temperature range. This mechanism may also involve the formation of "kebab" regions (lateral overgrowth on the "shish" structures) at relatively lower temperatures thereby having smaller long spacing than in the "shish" regions. The composite effect results in a compounded "tear-drop" scattering pattern. The "tear-drop" scattering pattern was also observed in the melt spun PVDF tapes [33], and injection molded polypropylene [34] and polyethylene [35]. As we move further towards the core at about 0.34–0.52 mm from the skin, we begin to see the third layer. The meridional spread of the intensity narrows resulting in the disappearance of the "tear-drop" pattern. The discrete scattering maxima gradually spread along the azimuthal direction as the distance from the surface increases. This is in accord with the WAXS observations confirming that the orientation levels persists well into the core region. The azimuthal intensity profile further proves that the population of the lamellae having their normal direction along the flow line is more than in the other directions resulting from the ellipsoidal spherulites (will be discussed in the companion paper on light scattering behavior of these materials) [30].

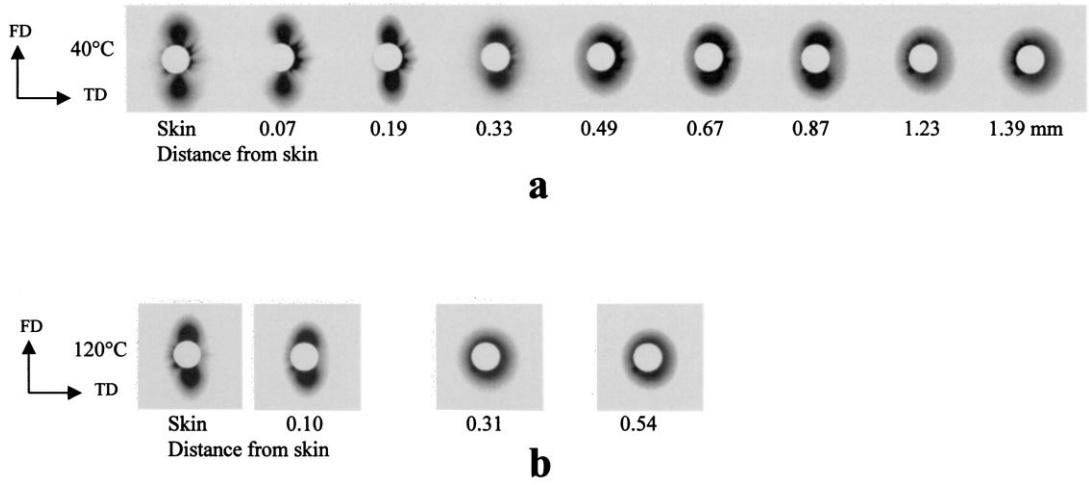

Fig. 16. SAXS patterns taken on microtomed thin slices (C cut) from skin to core for 85/15 (PVDF/PMMA) samples molded at 6.9 cm^3/s injection speed and at: (a) 40°C mold temperature; and (b) 120°C mold temperature.

When the mold temperature is increased to 120°C. The distinct scattering pattern observed in the skin layer of the sample molded at 40°C is not observable in this sample. This is probably because the skin layer of this sample is too thin, and the first layer cut out from this sample may have large portion of the shear zone. As a result, the first layer shows a "tear-drop" scattering pattern. We can also see from this figure that the thickness of the shear zone is much thinner compared to the sample molded at 40°C, and the position of the shear zone moves very close to the surface of the sample.

The long spacing of the crystallites can be calculated from the maximum scattering angle. The lamellae thickness and the interlamellar thickness can also be calculated from the long spacing data assuming a two phase model provided that the crystallinity data are available. Fig. 15 shows the long spacing calculated from the SAXS patterns for the above two samples along with the lamellae thickness and the interlamellar thickness data. The crystallinity data were reported in the first of this series of papers [29]. The sample molded at the higher mold temperature (120°C) shows overall larger long spacing and lamellae thickness than the sample molded at the lower mold temperature (40°C) due to its relatively higher crystallization temperature. The long spacing and the lamellae thickness increase with the increase of the distance from the surface for both samples.

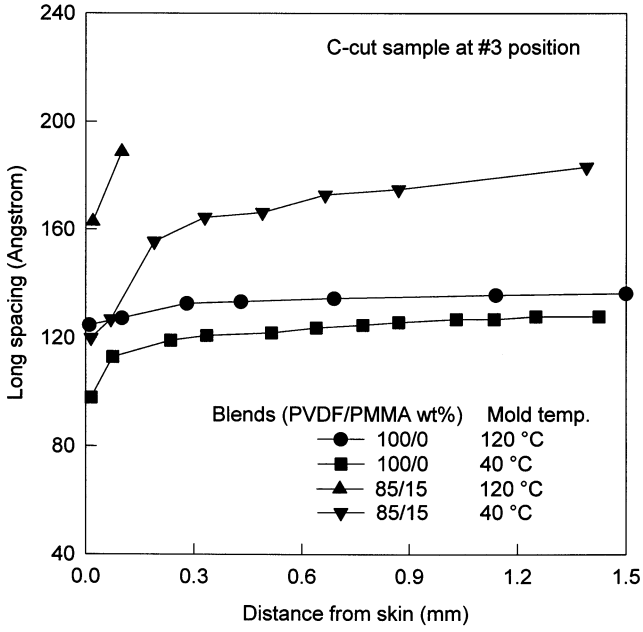

Fig. 17. Long spacing versus distance from skin for injection molded PVDF and PVDF/PMMA (85/15 wt%) at 40 and 120°C mold temperatures (injection flow rate of 6.9 cm^3/s).

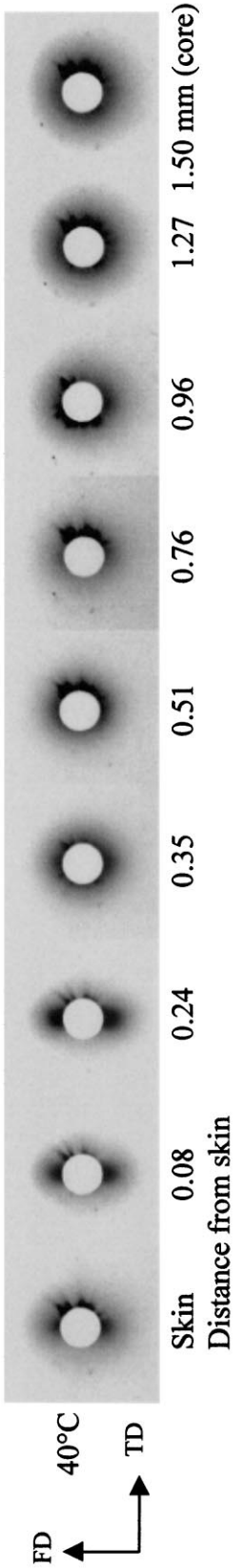

Fig. 18. SAXS patters taken on microtomed thin slices (C cut) from skin to core for 70/30 (PVDF/PMMA) samples molded at 6.9 cc/s injection speed and at 40°C mold temperature.

3.4.2. Injection molded blends of PVDF with PMMA

The SAXS patterns of the PVDF/PMMA (85/15 wt%) sample molded at 40°C mold temperature and at 6.9 cm^3/s injection flow rate are shown in Fig. 16a. In the skin and shear zone of this sample, the "tear-drop" shape scattering patterns from the shish–kebab crystalline structures are quite prevalent. At about 1.39 mm from the surface, the scattering pattern becomes isotropic indicating the presence of random lamellae orientation. In the core region the SAXS maxima are closer to the beam stop as compared to the 100% PVDF shown in Fig. 14a indicating that the overall structural modulation period for the PVDF/PMMA blend is longer than those of 100% PVDF sample.

Fig. 16b shows the SAXS patterns of the PVDF/PMMA (85/15 wt%) sample molded at 120°C and at 6.9 cm^3/s injection flow rate. Again we see the presence of the "tear-drop" scattering patterns in the skin layer and in the shear zone. Beyond about 0.31 mm from the skin the pattern becomes isotropic.

Long periods calculated from Figs. 14 and 16 are shown in Fig. 17. The value of LP starts small near the surface in all of the profiles. As expected, the sharpest gradient is exhibited in the samples molded at the low mold temperature where highest cooling rates are exhibited.

It should be noted that there is a significant increase in the long periods most possibly associated with the thickening of the amorphous regions by the inclusions of PMMA chains (or the exclusion of PMMA chains from the crystallizing domains).

With the addition of 30 wt% of PMMA, the scattering maxima move even closer to the beam stop appearing almost as a vertical streak at the skin layer with very small azimuthal spread as shown in Fig. 18. And this spread increases well into the shear region and beyond 0.35 mm isotropy prevails in these patterns. However, the long spacing data could not be calculated for this sample since the scattering maxima are too close to the beam stop. We were limited by the resolution of our X-ray camera.

4. Summary and conclusion

The skin layer of the injection molded PVDF/PMMA samples is formed under elongational flow. The data suggests that the skin regions are crystallized under high cooling rates and the crystallization took place in a relatively narrow temperature range. Lamella normals are primarily oriented in the FD. Although the crystalline orientation levels are relatively high at the surface, the highest crystalline orientation was found at a depth corresponding to the middle of the shear crystallized layer as detected by microbeam WAXS and WAXS pole figure techniques. In addition the SAXS data indicates that the shear crystallized regions exhibit very large distribution of long periods suggesting that the crystallization has taken place at a wide temperature range. The shear zone formed under the

shear flow possesses "shish–kebab" structure. The "shish" structure is formed under high shear stress early at elevated temperatures and the remainder of the crystalline regions including "kebab" lateral overgrowth that occurs at subsequent stages is formed at lower temperatures. The chain orientation starts relatively high at the skin and increases until the middle of the shear regions is reached and subsequently decreases reasonably monotonously towards the middle of the core. The use of higher injection speed and mold temperature retards the advancement of solidified layer development during injection thereby reducing the thickness of these layer(s) and the orientation levels developed within them. The local symmetry axes tilt inwards towards the core particularly at the interior portions of the shear crystallized layers.

The addition of small amount of diluent PMMA was found to enhance the chain orientation levels in the PVDF. This could be attributed to the increase of melt viscosity as well as reduction of "self" entanglements of the crystallizable PVDF chains. The addition of PMMA results in an increase in the long spacing due to the presence of the PMMA chains in the interlamellar regions. Beyond 30% PMMA content the molded parts were found to remain essentially amorphous when injection molded. A collective hierarchical structural model is presented in the companion paper where SALS and microbeam SALS techniques were employed to quantify the size and shape of crystallites and spherulites [30]. The overall structural interpretation taking into account WAXS, SAXS and SALS will be given at the end of the companion paper on SALS analysis [30].

References

[1] Ulcer Y, Cakmak M, Hsiung CM. J Appl Polym Sci 1995;55:1241.
[2] Hsiung CM, Cakmak M. J Appl Polym Sci 1993;47:125.
[3] Hsiung CM, Cakmak M. J Appl Polym Sci 1993;47:149.
[4] Hsiung CM, Cakmak M. Int Polym Process 1993;8:255.
[5] Ulcer Y, Cakmak M. Polymer 1997;38:2907.
[6] Ulcer Y, Cakmak M. J Appl Polym Sci 1996;62:1661.
[7] Ulcer Y, Cakmak M, Miao C, Hsiung CM. J Appl Polym Sci 1996;60:669.
[8] Keuchel K, Cakmak M. SPE ANTEC Tech Pap 1991;37:2477.
[9] White JL, Cakmak M. Int Polym Process 1987;2:48.
[10] Janeschitz-Kriegl H. Polymer melt rheology and flow birefringence. New York: Springer, 1983.
[11] Wales JLS, van Leeuwen J, van der Vijgh R. Polym Engng Sci 1972;12:358.
[12] Kamal MR, Tan V. Polym Engng Sci 1979;19:558.
[13] Chen SC, Chen YC. J Appl Polym Sci 1995;55(13):1757.
[14] Evans BL. J Mater Sci 1989;24(10):3588.
[15] Kadota M, Cakmak M, Hamada H. Polymer 1999;40:3119.
[16] Barret CS, Massalski TB. Structure of metals. 3rd ed. New York: McGraw Hill, 1966.
[17] Klug HP, Alexander LE. X-ray diffraction procedures for amorphous and polycrystalline materials. New York: Wiley, 1954 and 1976.
[18] Azaroff LV. Elements of X-ray crystallography. New York: McGraw Hill, 1968.
[19] Hahn T. International tables for crystallography. Dordrecht: Kluwer Academic, 1987.
[20] Hermans PH, Platzek P. Kolloid Z 1939;88:68.
[21] Stein RS. J Polym Sci 1958;31:327.
[22] White JL, Spruiell JE. Polym Engng Sci 1981;21:859.
[23] White JL. Pure Appl Chem 1983;55:765.
[24] White JL, Spruiell JE. Polym Engng Sci 1983;23:247.
[25] Keuchel K. Master thesis, The University of Akron, 1994.
[26] Alexander LE. X-ray diffraction method in polymer science. New York: Wiley, 1969.
[27] Mencik Z, Fitchmun DR. J Polym Sci, Polym Phys Ed 1973;11:973.
[28] Wu JP, White JL. Int Polym Process 1992;7:350.
[29] Wang YD, Cakmak M. J Appl Polym Sci 1998;68:909.
[30] Wang YD, Cakmak M. Polymer 2001;42:4233.
[31] Wilchinsky Z. J Appl Phys 1959;30:792.
[32] Wilchinsky Z. Advances in X-ray analysis, vol. 6. New York: Plenum Press, 1963 (p. 231).
[33] Cakmak M, Teitge A, Zachmann HG, White JL. J Polym Sci B 1993;31:371.
[34] Fujiyama M, Wakino T, Kawasaki Y. J Appl Polym Sci 1988;35:29.
[35] Rueda DR, Ania F, Lopez-Cabarcos E, Balta-Calleja FJ, Zachmann HG, Bayer RK. Polym Adv Technol 1991;2:57.